J|A|C|S ARTICLES

Published on Web 04/07/2010

Charge Generation and Recombination Dynamics in Poly(3-hexylthiophene)/Fullerene Blend Films with Different Regioregularities and Morphologies

Jiamo Guo,[†] Hideo Ohkita,*[,†,‡] Hiroaki Benten,[†] and Shinzaburo Ito[†]

Department of Polymer Chemistry, Graduate School of Engineering, Kyoto University, Katsura, Nishikyo, Kyoto 615-8510, Japan, and PRESTO, Japan Science and Technology Agency (JST), 4-1-8 Honcho Kawaguchi, Saitama 332-0012, Japan

Received January 13, 2010; E-mail: ohkita@photo.polym.kyoto-u.ac.jp

Abstract: The charge generation and recombination dynamics in blend films of a poly(3-hexylthiophene) (P3HT) and a methanofullerene derivative (PCBM) were comprehensively studied by transient absorption spectroscopy in the wavelength region from 450 to 1650 nm under various excitation intensities and different excitation wavelengths. In homogeneously mixed blend films of regiorandom P3HT (RRa-P3HT) and PCBM, virtually all the excitons can reach the interface of RRa-P3HT/PCBM and then form bound radical pairs. However, two-thirds of them geminately recombine to the ground state, and only one-third of them can be dissociated into free polarons that survive up to milliseconds. In phase-separated blend films of regioregular P3HT (RR-P3HT) and PCBM, almost all the excitons can reach the interface of RR-P3HT/PCBM, where most of them can be dissociated into free polarons efficiently and the rest of them form bound radical pairs. There are two pathways for the polaron generation: the prompt formation from hot excitons generated near the interface on a time scale of $<$100 fs and the delayed formation via the exciton migration to the interface on a time scale of $\sim$10 ps. The thermal annealing improves the charge dissociation efficiency of bound radical pairs. On the basis of such spectroscopic data, a series of fundamental photovoltaic conversion processes are quantitatively analyzed. Consequently, it is concluded that there is not much difference in the charge generation yield between RRa-P3HT/PCBM(50 wt %) and RR-P3HT/PCBM(50 wt %) blend films. Rather, the charge dissociation and collection have a critical impact on the overall device performance of P3HT/PCBM solar cells, where the phase-separated blend structures have a high tendency to form free carriers and transport these free carriers to the electrode.

1. Introduction

Polymer solar cells are attracting extensive academic and commercial interest for their potential applications to low-cost, lightweight, large-area, and flexible solar energy conversion platforms.[1,2] In particular, they have a great advantage in that they are suitable for simple solution processing, such as printing and coating technologies.[3−6] The photoactive layer of polymer solar cells is typically based on a bicontinuous blend of donor and acceptor materials, such as a conjugated polymer and a methanofullerene derivative, [6,6]-phenyl-C_{61}-butyric acid methyl ester (PCBM), thereby drastically maximizing the interface area where photogenerated excitons can be dissociated.[7,8] Recently, power conversion efficiencies in excess of 7% have been reported for a blend of a low-bandgap polymer and [70]PCBM ([6,6]-phenyl-C_{71}-butyric acid methyl ester).[9,10] Theoretical analyses have demonstrated that optimized polymer solar cells can have efficiencies of up to 10% for single cells and 15% for tandem cells.[1,11]

Regioregular poly(3-hexylthiophene) (RR-P3HT) and PCBM have been extensively studied as the most prominent materials in polymer solar cells, exhibiting reproducible efficiencies approaching 5% with relatively high external quantum efficiencies (>80%) and high fill factors ($\sim$0.7).[12−14] These device

[†] Kyoto University.
[‡] JST PRESTO.

(1) Dennler, G.; Scharber, M. C.; Brabec, C. J. *Adv. Mater.* **2009**, *21*, 1323–1338.
(2) Thompson, B. C.; Fréchet, J. M. J. *Angew. Chem., Int. Ed.* **2008**, *47*, 58–77.
(3) Yu, G.; Gao, J.; Hummelen, J. C.; Wudl, F.; Heeger, A. J. *Science* **1995**, *270*, 1789–1791.
(4) Halls, J. J. M.; Walsh, C. A.; Greenham, N. C.; Marseglia, E. A.; Friend, R. H.; Moratti, S. C.; Holmes, A. B. *Nature* **1995**, *376*, 498–500.
(5) Brabec, C. J.; Durrant, J. R. *MRS Bull.* **2008**, *33*, 670–675.
(6) Kim, J. Y.; Lee, K.; Coates, N. E.; Moses, D.; Nguyen, T.-Q.; Dante, M.; Heeger, A. J. *Science* **2007**, *317*, 222–225.
(7) Brabec, C. J.; Zerza, G.; Cerullo, G.; De Silvestri, S.; Luzzati, S.; Hummelen, J. C.; Sariciftci, S. *Chem. Phys. Lett.* **2001**, *340*, 232–236.
(8) Brabec, C. J.; Sariciftci, N. S.; Hummelen, J. C. *Adv. Funct. Mater.* **2001**, *11*, 15–26.
(9) Chen, H.-Y.; Hou, J.; Zhang, S.; Liang, Y.; Yang, G.; Yang, Y.; Yu, L.; Wu, Y.; Li, G. *Nat. Photonics* **2009**, *3*, 649–653.
(10) Liang, Y.; Xu, Z.; Xia, J.; Tsai, S.-T.; Wu, Y.; Li, G.; Ray, C.; Yu, L. *Adv. Mater.* **2010**, DOI: 10.1002/adma.200903528.
(11) Scharber, M. C.; Mühlbacher, D.; Koppe, M.; Denk, P.; Waldauf, C.; Heeger, A. J.; Brabec, C. J. *Adv. Mater.* **2006**, *18*, 789–794.
(12) Ma, W.; Yang, C.; Gong, X.; Lee, K.; Heeger, A. J. *Adv. Mater.* **2005**, *15*, 1617–1622.
(13) Li, G.; Shrotriya, V.; Huang, J.; Yao, Y.; Moriarty, T.; Emery, K.; Yang, Y. *Nat. Mater.* **2005**, *4*, 864–868.

10.1021/ja100302p

parameters are still the highest in organic solar cells. Most studies of the P3HT/PCBM blend devices have focused on the optimization of device performance through control of material properties such as regioregularity[14,15] and molecular weight[16] of P3HT, and fabrication conditions such as thermal annealing,[12,14,17,18] solvent annealing,[13,19] and additive processing.[20] All of these optimizations have a critical impact on phase-separated structures of P3HT and PCBM in the active layer. Recent morphological studies of the blend film have revealed the existence of three characteristic phases: fibrillar networks of P3HT crystals with typical widths of 13−15 nm, aggregates of PCBM nanocrystals, and relatively disordered P3HT matrices with PCBM nanocrystals.[21−23]

On the other hand, the molecular understanding of a series of fundamental processes[24,25] in polymer solar cells provides a clear guideline for improving the device performance effectively. Previous spectroscopic studies have provided information on the ultrafast formation of polarons in polymer/PCBM blend films.[7,26−31] For P3HT/PCBM blend films, the ultrafast charge transfer from P3HT to PCBM is on a time scale of <100 fs.[28−30] The charge transfer from PCBM to P3HT is also as fast as <250 fs.[31] Such an ultrafast charge-transfer rate is the origin of the charge-transfer efficiency as high as ∼100% at the interface of P3HT/PCBM in blend films.[8] Recently a near-infrared photoluminescence (PL) study[32] has shown that the PL intensity of the charge-transfer exciton in P3HT/PCBM blend films is strongly dependent on the regioregularities of P3HT, indicating that the geminate recombination of the charge-transfer exciton is closely related to the morphology of blend films. We also have recently reported that the photophysics in P3HT pristine films is strongly dependent on the regioregularities.[33] However, there are no systematic studies on the photophysics and photochemistry in P3HT/PCBM blend films in terms of the blend morphology depending on the regioregularities. Consequently, the fundamental processes in P3HT/PCBM blend films are not fully understood.

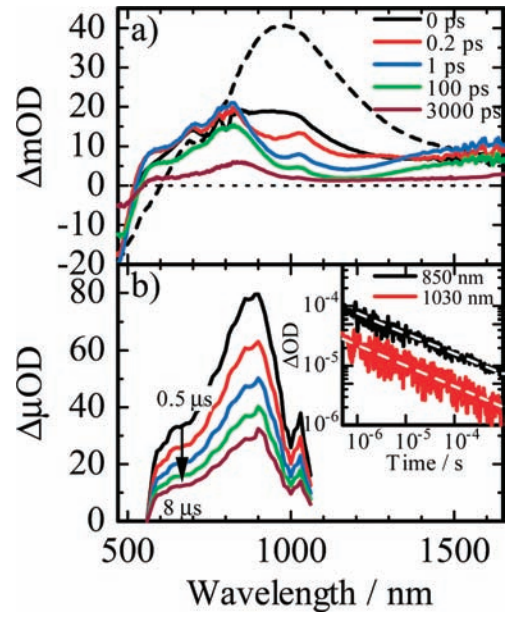

Figure 1. (a) Femtosecond transient absorption spectra of an RRa-P3HT pristine film (broken line) measured at 0 ps and RRa-P3HT/PCBM(50 wt %) blend films (solid lines) measured at 0, 0.2, 1, 100, and 3000 ps (from top to bottom). The excitation wavelength was 400 nm (∼30 μJ cm^{-2}). The transient absorption spectra were corrected for variation in the absorption at an excitation wavelength of 400 nm. (b) Microsecond transient absorption spectra of RRa-P3HT/PCBM(50 wt %) blend films measured at 0.5, 1, 2, 4, and 8 μs (from top to bottom). The inset shows transient absorption decays at 850 (upper) and 1030 nm (lower). The broken lines represent fitting curves with a power-law equation: $\Delta OD(t) \propto t^{-\alpha}$. The excitation wavelength was 450 nm (∼25 μJ cm^{-2}).

Herein we report a comprehensive spectroscopic study on the charge generation and recombination dynamics in P3HT/PCBM blend films with different regioregularities: RR-P3HT is employed as a model of a self-organized polymer, and RRa-P3HT is employed as a model of an amorphous polymer. We measured the femtosecond transient absorption of such blend films in the wavelength region from 450 to 1650 nm and quantitatively analyzed the efficiency of the following fundamental processes: the exciton diffusion to a donor/acceptor interface, the charge transfer at the interface, the charge dissociation into free carriers, and the charge collection to the electrodes. On the basis of these detailed analyses, we discuss the relevance of the fundamental processes we observed to the device performance of polymer solar cells.

2. Results

2.1. RRa-P3HT/PCBM. 2.1.1. Transient Absorption Spectra. Figure 1a shows the transient absorption spectra of RRa-P3HT pristine and RRa-P3HT/PCBM(50 wt %) blend films. As shown by the broken line, the RRa-P3HT pristine film exhibited a large absorption band around 1000 nm at 0 ps, which is ascribed to singlet excitons as reported previously.[33] On the other hand,

(14) Kim, Y.; Cook, S.; Tuladhar, S. M.; Choulis, S. A.; Nelson, J.; Durrant, J. R.; Bradley, D. D. C.; Giles, M.; McCulloch, I.; Ha, C.-S.; Ree, M. *Nat. Mater.* **2006**, *5*, 197–203.
(15) Woo, C. H.; Thompson, B. C.; Kim, B. J.; Toney, M. F.; Fréchet, J. M. J. *J. Am. Chem. Soc.* **2008**, *130*, 16324–16329.
(16) Hiorns, R. C.; de Bettignies, R.; Leroy, J.; Bailly, S.; Firon, M.; Sentein, C.; Khoukh, A.; Preud'homme, H.; Dagron-Lartigau, C. *Adv. Funct. Mater.* **2006**, *16*, 2263–2273.
(17) Erb, T.; Zhokhavets, U.; Gobsch, G.; Raleva, S.; Stühn, B.; Schilinsky, P.; Waldauf, C.; Brabec, C. J. *Adv. Funct. Mater.* **2005**, *15*, 1193–1196.
(18) Honda, S.; Nogami, T.; Ohkita, H.; Benten, H.; Ito, S. *ACS Appl. Mater. Interfaces* **2009**, *1*, 804–810.
(19) Li, G.; Yao, Y.; Yang, H.; Shrotriya, V.; Yang, G.; Yang, Y. *Adv. Funct. Mater.* **2007**, *17*, 1636–1644.
(20) Yao, Y.; Hou, J.; Xu, Z.; Li, G.; Yang, Y. *Adv. Funct. Mater.* **2008**, *18*, 1783–1789.
(21) Yang, X.; Loos, J.; Veenstra, S. C.; Verhees, W. J. H.; Wienk, M. M.; Kroon, J. M.; Michels, M. A. J.; Janssen, R. A. J. *Nano Lett.* **2005**, *5*, 579–583.
(22) van Bavel, S. S.; Sourty, E.; de With, G.; Loos, J. *Nano Lett.* **2009**, *9*, 507–513.
(23) Moon, J. S.; Lee, J. K.; Cho, S.; Byun, J.; Heeger, A. J. *Nano Lett.* **2009**, *9*, 230–234.
(24) Brédas, J.-L.; Norton, J. E.; Cornil, J.; Coropceanu, V. *Acc. Chem. Res.* **2009**, *42*, 1691–1699.
(25) Kippelen, B.; Brédas, J.-L. *Energy Environ. Sci.* **2009**, *2*, 251–261.
(26) Barbour, L. W.; Hegadorn, M.; Asbury, J. B. *J. Am. Chem. Soc.* **2007**, *129*, 15884–15894.
(27) Parkinson, P.; Lloyd-Hughes, J.; Johnston, M. B.; Herz, L. M. *Phys. Rev. B* **2008**, *78*, 115321.
(28) Hwang, I.-W.; Moses, D.; Heeger, A. J. *J. Phys. Chem. C* **2008**, *112*, 4350–4354.
(29) Piris, J.; Dykstra, T. E.; Bakulin, A. A.; van Loosdrecht, P. H. M.; Knulst, W.; Trinh, M. T.; Schins, J. M.; Siebbeles, L. D. A. *J. Phys. Chem. C* **2009**, *113*, 14500–14506.
(30) Marsh, R. A.; Hodgkiss, J. M.; Albert-Seifried, S.; Friend, R. H. *Nano Lett.* **2010**, *10*, 923–930.
(31) Cook, S.; Katoh, R.; Furube, A. *J. Phys. Chem. C* **2009**, *113*, 2547–2552.
(32) Hallermann, M.; Kriegel, I.; Como, E. D.; Berger, J. M.; von Hauff, E.; Feldmann, J. *Adv. Funct. Mater.* **2009**, *19*, 3662–3668.
(33) Guo, J.; Ohkita, H.; Benten, H.; Ito, S. *J. Am. Chem. Soc.* **2009**, *131*, 16869–16880.

the RRa-P3HT/PCBM blend film exhibited much smaller absorption bands around 800 and 1000 nm immediately after the laser excitation. Note that the negative signal around 500 nm is attributable to the photobleaching of the ground state of RRa-P3HT, which is indicative of the generation of photoexcitations such as excitons and polarons. The absorption signal at 1000 nm of the blend film measured at 0 ps was less than half that of the pristine film, which suggests that there exists a rapid quenching pathway such as charge generation, even on a time scale of <100 fs, in competition with rapid vibrational relaxation of the singlet exciton.[33] The singlet exciton band at 1000 nm decayed rapidly, and three absorption bands were distinctly observed at 800, 1030, and 1600 nm. The absorption peaks at 800 and 1600 nm red-shifted to 850 and >1600 nm with time, respectively, while that at 1030 nm remained the same. On a later time scale, as shown in Figure 1b, two absorption bands were observed at 900 and 1030 nm. Both bands exhibited power-law decay dynamics with an exponent of 0.35 over a long time range extending to milliseconds, as shown in the inset, suggesting trap-limited charge recombination between polymer polarons and PCBM anions.[34−36] The sharp absorption band at 1030 nm is ascribed to the PCBM anion, as we have reported previously.[37] The broad absorption bands at 800 and 1600 nm are thus ascribed to polymer polarons in RRa-P3HT, also consistent with the previous assignments.[38,39] Therefore, these findings suggest that polymer polarons and PCBM anions are promptly generated even at 0 ps, and some of them survive up to the millisecond time domain, as discussed later.

2.1.2. Charge Generation. To study the charge generation dynamics in RRa-P3HT/PCBM blend films in more detail, we measured the time evolution of transient absorption signals in the earlier time domain up to 1 ps. As shown in Figure 2a, the time evolution of transient absorption signals at 1600 nm was well fitted with a monoexponential rise (0.24 ps, 32%) and a constant fraction (68%). As mentioned above, this band is safely ascribed to the polymer polaron band because it can be observed separately. On the other hand, the transient signals at 1000 nm are due to a superposition of polymer singlet excitons, polymer polarons, and PCBM anions in an earlier time domain, as shown in Figure 1a, but can be ascribed to only polymer polarons and PCBM anions at 1 ps. To extract the singlet exciton decay, we subtract the transient signals at 1600 nm (closed triangles) from those at 1000 nm (solid line): both signals are normalized at 1 ps. The extracted transient signals at 1000 nm (closed circles) were well fitted with an exponential function with a decay constant of 0.23 ps, which is in good agreement with the rise constant of the polymer polaron band. This agreement suggests that polymer polarons are not only promptly generated during the laser excitation (<100 fs) but also rapidly generated with a time constant of ∼0.2 ps from polymer singlet excitons. Furthermore, as shown in Figure 2b, no change in the ground-state photobleaching signals at 470 nm was observed on a time scale of <1 ps, indicating that no photoexcitations such as singlet excitons return to the ground state. In other words, all of the singlet excitons are separated into polymer polarons and PCBM anions: the charge generation efficiency is as high as ∼100%. Note that triplet formation can be ruled out because of the slow intersystem crossing rate (∼1 ns^{-1}) for polythiophene.[40] This finding is consistent with the high efficiency in the PL quenching ($\Phi_q \approx 100\%$, see the Supporting Information). The transient absorption dynamics at 470 and 1000 nm were independent of the excitation intensities ranging from 6 to 120 $\mu J\ cm^{-2}$ (see the Supporting Information), suggesting that both charge generation processes (<100 fs, ∼0.2 ps) are much faster than other rapid competitive relaxations such as singlet exciton−exciton annihilation reported for pristine films.[33,41,42]

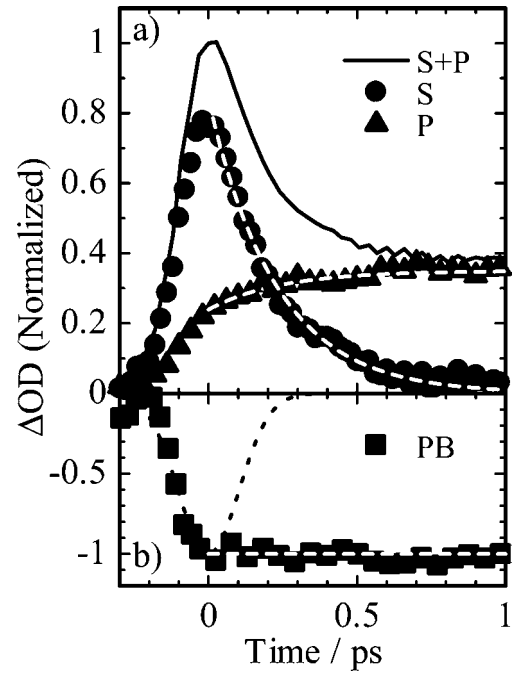

Figure 2. Normalized femtosecond transient absorption signals at (a) 1000 nm (singlet exciton and polaron, S+P; solid line) and (b) 470 nm (photobleaching, PB; closed squares) of RRa-P3HT/PCBM(50 wt %) blend films excited at 400 nm (∼30 $\mu J\ cm^{-2}$). The closed circles show the decay fraction at 1000 nm (singlet exciton, S) that is evaluated by subtracting the transient absorption signal of RRa-P3HT polarons at 1600 nm (P, closed triangles) from that at 1000 nm: both signals are normalized at 1 ps. The subtracted transient absorption signal (closed circles) was fitted with a monoexponential function: $\Delta OD(t) = A_D \exp(-t/\tau_D)$. The transient absorption rise at 1600 nm was fitted with an exponential function and a constant: $\Delta OD(t) = A_R[1 - \exp(-t/\tau_R)] + B$. The transient absorption signal at 470 nm was fitted with a constant: $\Delta OD(t) =$ constant. The broken lines represent the best-fitting curves. The dotted line indicates the instrument response function of the femtosecond transient absorption spectroscopy.

2.1.3. Charge Recombination and Dissociation. To study the charge recombination dynamics in RRa-P3HT/PCBM blend films, we measured the decay dynamics of three transient signals on a time scale of nanoseconds: the ground-state photobleaching (480 nm), RRa-P3HT polarons (850 nm), and PCBM anion (1030 nm). Here we quantitatively analyzed the decay dynamics at 480 and 1030 nm under a low excitation intensity of 12 μJ

(34) Nogueira, A. F.; Montanari, I.; Nelson, J.; Durrant, J. R.; Winder, C.; Sariciftci, N. S.; Brabec, C. *J. Phys. Chem. B* **2003**, *107*, 1567–1573.
(35) Nelson, J. *Phys. Rev. B* **2003**, *67*, 155209.
(36) Ohkita, H.; Cook, S.; Astuti, Y.; Duffy, W.; Tierney, S.; Zhang, W.; Heeney, M.; McCulloch, I.; Nelson, J.; Bradley, D. D. C.; Durrant, J. R. *J. Am. Chem. Soc.* **2008**, *130*, 3030–3042.
(37) Yamamoto, S.; Guo, J.; Ohkita, H.; Ito, S. *Adv. Funct. Mater.* **2008**, *18*, 2555–2562.
(38) Österbacka, R.; An, C. P.; Jiang, X. M.; Vardeny, Z. V. *Science* **2000**, *287*, 839–842.
(39) Jiang, X.; Österbacka, R.; Korovyanko, O.; An, C. P.; Horovitz, B.; Janssen, R. A. J.; Vardeny, Z. V. *Adv. Funct. Mater.* **2002**, *12*, 587–597.
(40) Kraabel, B.; Moses, D.; Heeger, A. J. *J. Chem. Phys.* **1995**, *103*, 5102–5108.
(41) Dogariu, A.; Vacar, D.; Heeger, A. J. *Phys. Rev. B* **1998**, *58*, 10218–10224.
(42) Watanabe, S.; Furube, A.; Katoh, R. *J. Phys. Chem. A* **2006**, *110*, 10173–10178.

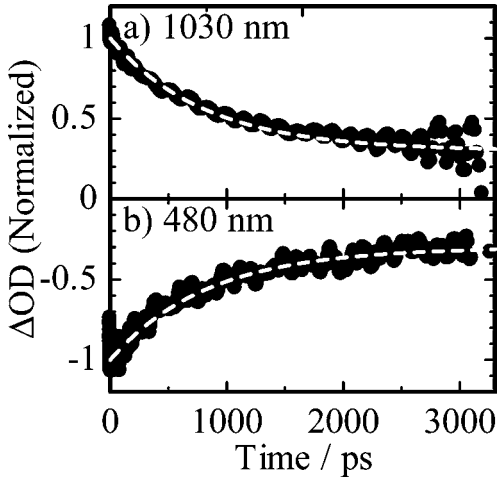

Figure 3. Normalized femtosecond transient absorption decays of RRa-P3HT/PCBM(50 wt %) blend films excited at 400 nm (~12 μJ cm^{-2}), measured at (a) 1030 and (b) 480 nm. The transient absorption decays were fitted with an exponential function and a constant: $\Delta OD(t) = A_D \exp(-t/\tau_D) + B$. The broken lines represent the best-fitting curves.

cm^{-2}, because the decay dynamics at 850 nm is the same as that at 1030 nm. As shown in Figure 3a, the transient absorption decay of the PCBM anion was fitted with an exponential function (813 ps, 69%) and a constant fraction (31%). On the other hand, as shown in Figure 3b, the photobleaching signals were also fitted with an exponential function (835 ps, 69%) and a constant fraction (31%). Furthermore, the decay dynamics of the RRa-P3HT polarons, the PCBM anion, and the ground-state photobleaching was independent of the excitation intensities ranging from 6 to 120 μJ cm^{-2}, suggesting monomolecular decay such as geminate recombination of bound radical pairs (see the Supporting Information). Therefore, the agreement in the time constant and the fraction shows that the decay component can be ascribed to the geminate recombination of polymer polarons and PCBM anions leading to the recovery to the ground state. On the other hand, the constant component is ascribed to dissociated free carriers, which would survive over the millisecond time scale, as shown in Figure 1b.

2.2. RR-P3HT/PCBM. 2.2.1. Transient Absorption Spectra. Figure 4 shows the transient absorption spectra of RR-P3HT pristine and RR-P3HT/PCBM(5−50 wt %) blend films. As shown by the broken line in Figure 4a, the RR-P3HT pristine film exhibited a large absorption band around 1200 nm at 0 ps, which is ascribed to singlet excitons as reported previously.[33] On the other hand, the RR-P3HT/PCBM blend films exhibited a smaller absorption band around 1200 nm immediately after the laser excitation at 400 nm. Note that the negative signal around 500 nm is attributable to the photobleaching of the ground state of RR-P3HT, which is again indicative of the generation of photoexcitations such as excitons and polarons. At a later time stage, the singlet exciton band disappeared, and instead broad absorption bands were observed from 700 to 1000 nm. These bands decayed slowly and were hence observed even on a time scale of milliseconds (see the Supporting Information). We have previously ascribed these bands to polymer polarons in RR-P3HT because they exhibited power-law decay dynamics over a long time range extending to milliseconds.[43] As shown in parts a−c of Figure 4, the singlet exciton band decreased

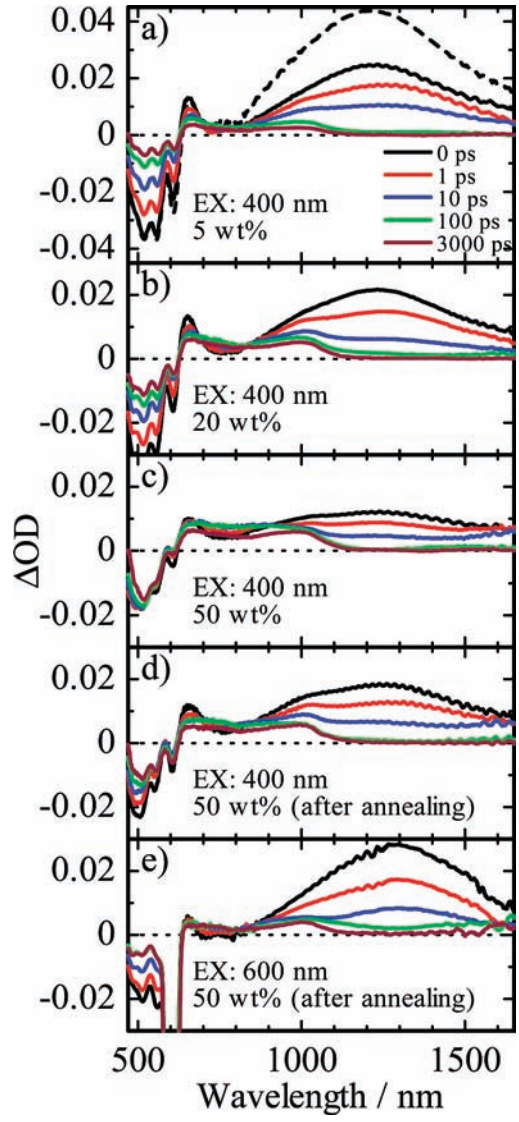

Figure 4. Femtosecond transient absorption spectra of an RR-P3HT pristine film (broken line in panel a) measured at 0 ps and (a−e) RR-P3HT/PCBM(5−50 wt %) blend films (solid lines) measured at 0, 1, 10, 100, and 3000 ps (from top to bottom in each panel). The excitation wavelengths were (a−d) 400 nm (~15 μJ cm^{-2}) and (e) 600 nm (~10 μJ cm^{-2}). The PCBM concentrations were (a) 5, (b) 20, and (c−e) 50 wt %. The spectra in panels d and e were measured after thermal annealing at 140 °C for 30 min. The transient absorption spectra were corrected for variation in the absorption at the excitation wavelengths.

and the polaron bands increased with increasing PCBM concentration, suggesting that the formation yield of polymer polarons is dependent on the blend morphology. Figure 4d shows the transient absorption spectra of the RR-P3HT/PCBM(50 wt %) blend film after thermal annealing at 140 °C for 30 min. The singlet exciton band at 0 ps slightly increased, suggesting that some excitons cannot reach the P3HT/PCBM interface because of the enlargement of P3HT domains due to thermal annealing. This is consistent with the PL quenching result as mentioned below. The ground-state photobleaching spectra were also dependent on the PCBM concentration: the bleaching peak at 610 nm, which corresponds to the absorption shoulder in the ground-state absorption indicating the crystallization of RR-P3HT, was less distinguished at higher PCBM concentrations and before thermal annealing. Analysis of the polymer polaron bands from 700 to 1000 nm in more detail

(43) Guo, J.; Ohkita, H.; Benten, H.; Ito, S. *J. Am. Chem. Soc.* **2009**, *131*, 16869–16880.

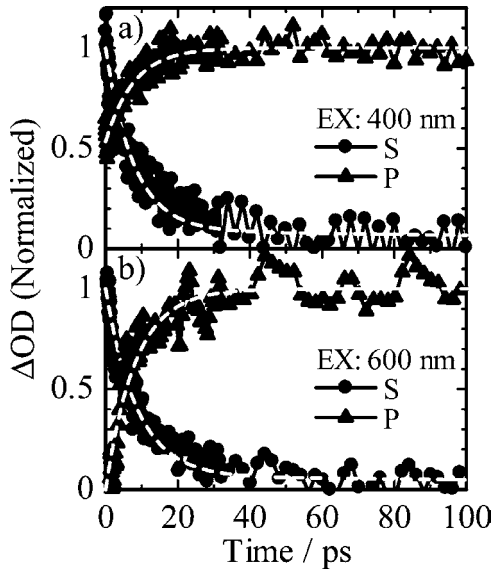

Figure 5. Normalized femtosecond transient absorption signals of RR-P3HT/PCBM(50 wt %) blend films after thermal annealing measured at 1200 nm (singlet exciton, S; closed circles) and 1000 nm (polaron, P; closed triangles). The excitation wavelengths were (a) 400 nm ($\sim$15 μJ cm^{-2}) and (b) 600 nm ($\sim$10 μJ cm^{-2}). The rise signals at 1000 nm were evaluated by subtracting the transient absorption signals of singlet excitons at 1200 nm from that at 1000 nm (see the Supporting Information). The transient absorption decay at 1200 nm was fitted with a sum of two exponential functions: $\Delta OD(t) = A_{D1} \exp(-t/\tau_{D1}) + A_{D2} \exp(-t/\tau_{D2})$. The subtracted transient absorption signal at 1000 nm was fitted with an exponential function and a constant: $\Delta OD(t) = A_R[1 - \exp(-t/\tau_R)] + B$. The broken lines represent the best-fitting curves.

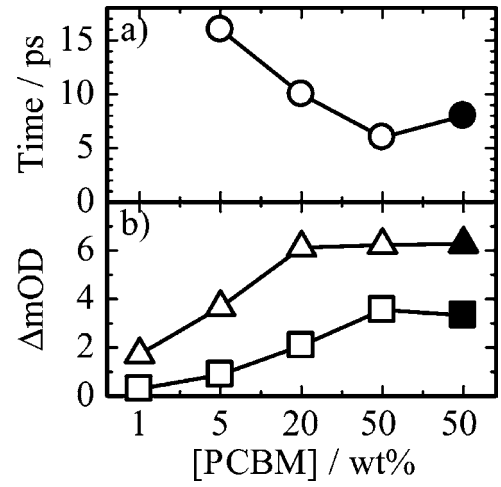

Figure 6. (a) Time constants (circles) for singlet exciton decay and polaron formation in RR-P3HT/PCBM(5−50 wt %) blend films plotted against the PCBM concentration. The time constants were obtained from the fitting of the transient absorption decays at 1200 nm and the transient absorption rises at 1000 nm. (b) Transient absorption signals for polarons observed at 1000 nm in RR-P3HT/PCBM(1−50 wt %) blend films plotted against the PCBM concentration. The constant fraction B of the fitting function, $\Delta OD(t) = A_R[1 - \exp(-t/\tau_R)] + B$, was plotted as the prompt transient absorption signals (<100 fs, squares). The total transient absorption signals (triangles) were obtained from $A_R + B$, where A_R is the delayed transient absorption signals ($\sim$10 ps). The open and closed symbols represent the values measured before and after thermal annealing, respectively. The transient absorption signals were corrected for variation in the absorption at an excitation wavelength of 400 nm.

revealed that transient absorption signals around 800 nm increased with increasing PCBM concentration on a time scale of sub-nanoseconds. This absorption is different from that of polaron bands at 700 and 1000 nm observed for RR-P3HT/PCBM blend films on the microsecond time scale but is rather similar to the polaron band at 800 nm observed for the amorphous blend film of RRa-P3HT/PCBM, as mentioned above. To excite the crystalline domain of RR-P3HT selectively, we measured the transient absorption spectra of RR-P3HT/PCBM(50 wt %) blend films after thermal annealing upon excitation at 600 nm. As shown in Figure 4e, the absorption spectrum at 0 ps was different from those of blend films excited at 400 nm, but rather similar to that of an RR-P3HT pristine film, suggesting that no polarons are generated immediately after the laser excitation. We will discuss later the formation mechanism of polymer polarons in terms of the crystallinity of P3HT.

2.2.2. Charge Generation. To address the charge generation mechanism in RR-P3HT/PCBM blend films, we measured the decay of singlet excitons at 1200 nm and the formation of polarons at 1000 nm upon excitation at 400 and 600 nm. As mentioned above, the transient signal at 1200 nm is safely ascribed to the polymer singlet exciton band on a time scale of sub-nanoseconds. On the other hand, the transient signals at 1000 nm are due to a superposition of polymer singlet excitons, polymer polarons, and PCBM anions in this time domain. We therefore subtract the decay fraction of singlet excitons from the transient signals at 1000 nm to extract the formation dynamics of polarons. Details are given in the Supporting Information. Figure 5 shows the time evolution of the decay of singlet excitons at 1200 nm and the formation of polarons at 1000 nm in RR-P3HT/PCBM(50 wt %) blend films after thermal annealing. For singlet excitons, the transient absorption decays at 1200 nm were fitted independently of the excitation wavelength with a sum of two exponential functions: $\Delta OD(t) = A_{D1} \exp(-t/\tau_{D1}) + A_{D2} \exp(-t/\tau_{D2})$. The longer lifetime τ_{D2} was fixed to a PL lifetime of 330 ps to represent the monomolecular decay dynamics of RR-P3HT singlet excitons.[33] The shorter lifetime was evaluated to be $\sim$8 ps, which was independent of the excitation wavelength. For polarons, the formation dynamics of polarons at 1000 nm was fitted with a monoexponential rise and a constant fraction. The rise time constant was evaluated to be $\sim$8 ps, which was also independent of the excitation wavelength. The agreement in the decay and rise time constants of singlet excitons and polarons strongly suggests that polarons are generated from singlet excitons. Interestingly, there was a constant fraction of $\sim$53% for the excitation at 400 nm but no constant fraction for the excitation at 600 nm. In other words, there are two pathways for the polaron generation upon excitation at 400 nm: half of the polarons are promptly generated on a time scale of <100 fs, and the other half are generated on a time scale of tens of picoseconds. On the other hand, there is only one pathway for the polaron generation upon excitation at 600 nm, which corresponds to the absorption shoulder due to the crystallization of RR-P3HT.

To further understand the origin of the two pathways for the polaron generation in the RR-P3HT/PCBM blend films, we analyzed the transient dynamics of RR-P3HT/PCBM blend films with different PCBM concentrations in the same way. As shown in Figure 6a, the rise and decay constants for polarons and singlet excitons (open circles) decreased from 16 to 6 ps with increasing PCBM concentration from 5 to 50 wt %, and slightly increased to 8 ps (closed circles) after thermal annealing at a PCBM concentration of 50 wt %. Figure 6b shows the formation yields of polarons in RR-P3HT/PCBM blend films. The triangles are the saturated ΔOD in the formation dynamics of polarons

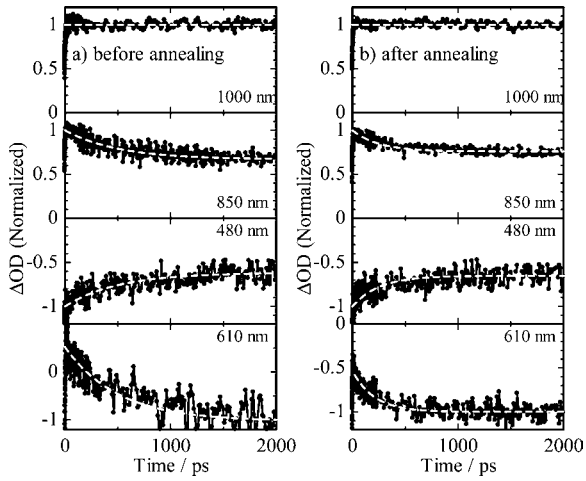

Figure 7. Normalized femtosecond transient absorption signals of RR-P3HT/PCBM(50 wt %) blend films (a) before and (b) after thermal annealing excited at 400 nm (~12 μJ cm^{-2}), measured at 850, 1000, 480, and 610 nm. The transient absorption decays at 850 and 480 nm were fitted with an exponential function and a constant: $\Delta OD(t) = A_D \exp(-t/\tau_D) + B$. The transient absorption rises at 610 nm were fitted with an exponential function and a constant: $\Delta OD(t) = A_R[1 - \exp(-t/\tau_R)] + B$. The transient absorption signals at 1000 nm were fitted with a constant: $\Delta OD(t) =$ constant. The broken lines represent the best-fitting curves.

as shown in Figure 5, which represent the total formation yield of polarons. The squares are the initial ΔOD at 0 ps, which represent the prompt formation of polarons on a time scale of <100 fs. Thus, the difference between them represents the delayed formation of polarons on a time scale of 6−16 ps. As shown in Figure 6b, the prompt formation of polarons is negligible at PCBM concentrations lower than 1 wt % but increases with increasing PCBM concentration and consequently accounts for ~57% of the polaron formation at a PCBM concentration of 50 wt %. After thermal annealing, the prompt formation slightly decreased to ~53%. The dependence of polaron yields on the PCBM concentration is qualitatively consistent with the PL quenching measurement: Φ_q increased from ~78 to ~95% with increasing PCBM concentration from 5 to 50 wt % and slightly decreased to ~91% after thermal annealing (see the Supporting Information). These findings suggest that the polaron yield in RR-P3HT/PCBM is strongly dependent on the blend morphology, as discussed later.

2.2.3. Charge Recombination and Dissociation. We now turn to analyze the charge recombination dynamics in RR-P3HT/PCBM(50 wt %) blend films before and after thermal annealing. Figure 7 shows the time evolution of the polaron bands at 850 and 1000 nm and the photobleaching signals at 480 and 610 nm under a low excitation intensity of 12 μJ cm^{-2}, where the bimolecular recombination is negligible (see the Supporting Information). As shown in Figure 7a, the polaron band at 1000 nm kept constant in the nanosecond time domain. Note that the decay dynamics of the 700 nm band is the same as that of the 1000 nm band (see the Supporting Information). In contrast, the polaron band at 850 nm decayed monoexponentially with a lifetime of ~500 ps (33%) and a constant fraction (67%). The photobleaching signals at 480 and 610 nm were also fitted with an exponential decay or rise fraction with a time constant of ~500 ps and a constant fraction. As mentioned above, the polaron band at 850 nm is similar to the polaron band observed for amorphous blend films of RRa-P3HT/PCBM. The photobleaching signal at 480 nm is also mainly attributed to the absorption of amorphous P3HT, because RRa-P3HT pristine films exhibit an absorption band around 435 nm. On the other hand, the photobleaching signal at 610 nm is only attributed to the absorption of crystalline P3HT, which is characteristic of $\pi-\pi$ stacking of RR-P3HT (see the Supporting Information).[44,45] Therefore, these findings suggest that polymer polarons migrate from amorphous domains to crystalline domains in RR-P3HT/PCBM blend films, as discussed later. After thermal annealing, as shown in Figure 7b, RR-P3HT/PCBM blend films exhibited faster decay or rise dynamics compared to that before thermal annealing. The transient absorption decay at 850 nm was fitted with an exponential fraction with a lifetime of ~250 ps (24%) and a constant fraction (76%). The photobleaching signals at 480 and 610 nm were also fitted with an exponential decay or rise fraction with a time constant of ~250 ps and a constant fraction. These results suggest that the hole migration is enhanced by thermal annealing.

3. Discussion

3.1. Assignments of Polarons. We first summarize various P3HT polarons generated in P3HT/PCBM blend films before discussing the photophysics in these films in detail. For RRa-P3HT/PCBM blend films, as shown in Figure 1, two absorption bands at ~800 and 1600 nm are mainly assigned to relatively localized polarons bound to PCBM anions in RRa-P3HT amorphous domains[46,47] because their monomolecular decay is indicative of geminate recombination. The 800- and 1600-nm bands can be attributed to a transition from the SOMO to the LUMO (P_2 transition) and a transition from the HOMO to the SOMO (P_1 transition), respectively, consistent with previous reports on polythiophenes.[38,39,48,49] As mentioned above, the 850-nm band is red-shifted to 900 nm on a time scale of microseconds. This red-shift is probably due to the stabilization of polarons by hole migration or structural relaxation of polarons. For RR-P3HT/PCBM blend films with lower PCBM concentrations (<20 wt %), as shown in Figure 4, two absorption bands around 700 and 1000 nm are observed. Previously, we reported that RR-P3HT pristine films have an absorption band at 650 nm with a lifetime of a few picoseconds, and we assigned it to polaron pairs of polymer cation and anion.[33] In RR-P3HT/PCBM blend films, as shown in Figure 4, the same absorption band is observed at an earlier time stage but rapidly decays in a few picoseconds. On the other hand, we recently reported that RR-P3HT/PCBM blend films have two absorption bands at 700 and 1000 nm on a time scale of microseconds, and we assigned the 700-nm band to delocalized polarons in crystalline domains and the 1000-nm band to localized polarons in disordered domains.[43] We therefore assign the 700- and 1000-nm bands observed on a time scale from tens of picoseconds to nanoseconds to delocalized polarons and localized polarons, respectively. These assignments are also consistent with previous

(44) Brown, P. J.; Thomas, D. S.; Köhler, A.; Wilson, J. S.; Kim, J.-S.; Ramsdale, C. M.; Sirringhaus, H.; Friend, R. H. *Phys. Rev. B* **2003**, *67*, 064203.
(45) Zhokhavets, U.; Erb, T.; Gobsch, G.; Al-Ibrahim, M.; Ambacher, O. *Chem. Phys. Lett.* **2006**, *418*, 347–350.
(46) Chen, T.-A.; Wu, X.; Rieke, R. D. *J. Am. Chem. Soc.* **1995**, *117*, 233–244.
(47) Hugger, S.; Thomann, R.; Heinzel, T.; Thurn-Albrecht, T. *Colloid Polym. Sci.* **2004**, *282*, 932–938.
(48) Beljonne, D.; Cornil, J.; Sirringhaus, H.; Brown, P. J.; Shkunov, M.; Friend, R. H.; Brédas, J.-L. *Adv. Funct. Mater.* **2001**, *11*, 229–234.
(49) Sirringhaus, H.; Brown, P. J.; Friend, R. H.; Nielsen, M. M.; Bechgaard, K.; Langeveld-Voss, B. M. W.; Spiering, A. J. H.; Janssen, R. A. J.; Meijer, E. W.; Herwig, P.; de Leeuw, D. M. *Nature* **1999**, *401*, 685–688.

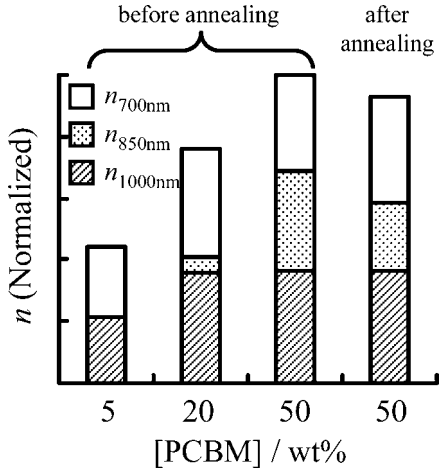

Figure 8. Normalized relative polaron densities (n) of delocalized polarons at 700 nm ($n_{700\ nm}$), localized polarons at 1000 nm ($n_{1000\ nm}$), localized polarons bound to PCBM anions at 850 nm ($n_{850\ nm}$), and total polarons formed in RR-P3HT/PCBM(5−50 wt %) blend films plotted against the PCBM concentration before and after thermal annealing. The polaron densities are normalized at the total polaron density of RR-P3HT/PCBM(50 wt %) blend films before thermal annealing.

reports on polythiophenes.[38,39,48,49] Interestingly, RR-P3HT/PCBM(50 wt %) blend films exhibit a new absorption around 800 nm besides the 700- and 1000-nm bands on the sub-nanosecond time scale upon excitation at 400 nm. As mentioned above, this band at 800 nm is rather similar to the polaron band of RRa-P3HT/PCBM blend films, suggesting that this is due to localized polarons bound to PCBM anions in disordered amorphous domains. We therefore conclude that the 800-nm absorption is ascribed to the P_2 transition of localized polarons bound to PCBM anions in disordered amorphous P3HT domains in RR-P3HT/PCBM(50 wt %) blend films because of high PCBM concentrations. The relative energy levels for polarons generated in P3HT/PCBM blend films and their transition energies are summarized in the Supporting Information. For the quantitative discussion, we analyze the polaron density on the basis of the molar absorption coefficient of each polaron. The molar absorption coefficient of RRa-P3HT polarons bound to PCBM anions was evaluated to be 2.0×10^4 M^{-1} cm^{-1} at 850 nm from comparison with that of PCBM anions (6×10^3 M^{-1} cm^{-1} at 1020 nm).[37] We assume that the 800-nm band observed for RR-P3HT/PCBM(50 wt %) blend films has the same molar absorption coefficient as the RRa-P3HT bound polaron band. Recently we evaluated the molar absorption coefficients of the other polarons to be 3.5×10^4 M^{-1} cm^{-1} for delocalized polarons at 700 nm and 3.0×10^4 M^{-1} cm^{-1} for localized polarons at 1000 nm.[43] From the spectral simulation to Figure 4 based on these absorption spectra and molar absorption coefficients, we evaluate the relative polaron densities at 100 ps when all the polarons are generated and their decay is negligible or limited. Details are given in the Supporting Information. As shown in Figure 8, the total polaron density increases with increasing PCBM concentration. After thermal annealing of the RR-P3HT/PCBM(50 wt %) blend film, the total density slightly decreases. This is due to the formation of larger phase-separated polymer domains by thermal annealing. Interestingly, localized bound polarons at 850 nm in disordered amorphous domains are negligible in RR-P3HT/PCBM blend films with lower concentrations of PCBM(<20 wt %) but increase to 33% in RR-P3HT/PCBM(50 wt %) blend films before thermal annealing and slightly decrease to 24% after thermal annealing. This finding demonstrates that P3HT polarons generated in RR-P3HT/PCBM blend films are closely related to the film morphology. Recent studies have shown that there are three phases in RR-P3HT/PCBM blend films: fibrillar network of P3HT crystals, aggregates of PCBM nanocrystals, and relatively disordered P3HT matrices with PCBM nanocrystals.[21−23] We therefore speculate, as illustrated in Scheme 1, that delocalized polarons at 700 nm are located in fibrillar networks of P3HT crystals, localized polarons at 1000 nm are located in disordered P3HT matrices, and localized polarons at 850 nm are loosely bound to PCBM at the interface in disordered amorphous P3HT matrices.

Scheme 1. Schematic Illustration of Charge Generation Mechanisms in Phase-Separated Structures of RR-P3HT/PCBM(50 wt %) Blend Films[a]

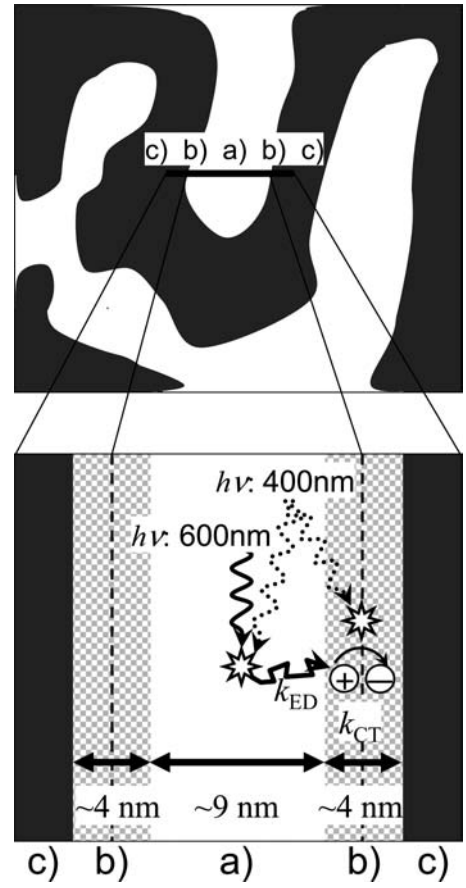

[a] The upper figure shows phase-separated structures of RR-P3HT and PCBM blend films taken from ref 23: the widths of RR-P3HT and PCBM domains and ~13 and ~11 nm, respectively. The lower figure shows an enlarged local area of the top figure based on our transient study: (a) the core P3HT crystals, (b) the disordered P3HT and PCBM, and (c) the PCBM crystals. The broken lines indicate the center of the RR-P3HT/PCBM interface. The charge transfer (k_{CT}) is on a time scale of <100 fs at the interface with a width of ~4 nm, corresponding to the delocalization radius of singlet excitons excited at 400 nm. The singlet excitons generated at the core P3HT crystals result in polaron formation after exciton migration (k_{ED}) to the interface.

3.2. Exciton Diffusion and Charge Generation. In RRa-P3HT/PCBM(50 wt %) blend films, as shown in Figure 2, ~65% of polarons are generated promptly on a time scale of <100 fs, and ~35% of polarons are generated with a time constant of ~0.2 ps. Such rapid formation of polarons is ascribed to the charge generation at the interface of RRa-P3HT and PCBM, because the exciton migration is negligible on such a short time scale, <0.2 ps. This is probably because most of the

Scheme 2. Energy Diagrams of Fundamental Photovoltaic Conversion Processes in P3HT/PCBM Solar Cells[a]

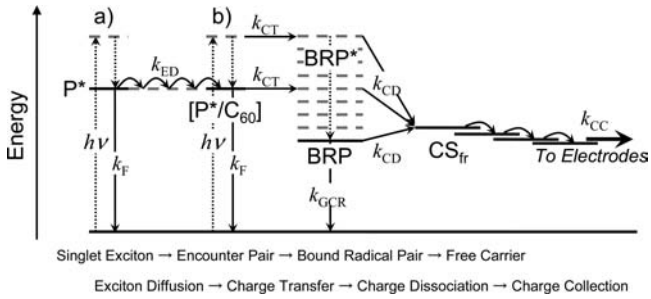

[a] The energy levels involved in photovoltaic conversion are as follows: P*, singlet exciton (a, P3HT crystalline domain; b, P3HT/PCBM interface); [P*/C_{60}], encounter pair; BRP*, nonrelaxed bound radical pair; BRP, relaxed bound radical pair; CS_{fr}, free carrier. The fundamental processes for photovoltaic conversion are as follows: $h\nu$, light absorption; k_F, total monomolecular deactivations of singlet excitons in P3HT pristine films; k_{ED}, singlet exciton diffusion to the P3HT/PCBM interface and formation of encounter pair; k_{CT}, charge transfer from P3HT to PCBM; k_{GCR}, geminate recombination of bound radical pair; k_{CD}, charge dissociation from bound radical pair; k_{CC}, charge collection of free carriers. Note that in the RRa-P3HT/PCBM(50 wt %) blend films, the exciton diffusion is negligible because of the homogeneously mixed structures.

PCBM molecules are homogeneously dispersed in the RRa-P3HT amorphous matrix, which would result in an intermolecular distance less than 1 nm. Previously we estimated the delocalization radius of singlet excitons (3.2 nm) in the RRa-P3HT film.[33] This is longer than the estimated intermolecular distance, suggesting that singlet excitons can encounter a PCBM molecule without exciton migration, as shown in Scheme 2b. Furthermore, as shown in Figure 2b, no singlet excitons return to the ground state during the time scale of the charge separation. We therefore conclude that both the exciton diffusion efficiency (η_{ED}) and the charge-transfer efficiency (η_{CT}) are as high as 100% in RRa-P3HT/PCBM(50 wt %) blend films.

In RR-P3HT/PCBM blend films, as mentioned above, there are two pathways for the polaron generation upon excitation at 400 nm: the prompt formation of polarons on a time scale of <100 fs and the delayed formation of polarons on a time scale of 6−16 ps. The prompt formation of polarons is as fast as the vibrational relaxation. In the RR-P3HT bulk, hot-exciton dissociation would be involved. Previous studies have shown that the dissociation of hot excitons can generate polarons in the RR-P3HT bulk.[29,33,50−52] If this mechanism were dominant, the yield of the prompt formation should decrease with increasing PCBM concentration because of the decrease in the P3HT bulk domains. As shown in Figure 6, this is not the case. The increase in the prompt polaron formation is rather ascribed to a larger interface area in RR-P3HT/PCBM blend films with increasing PCBM concentration. The yield of the prompt polaron formation slightly decreases after thermal annealing of RR-P3HT/PCBM(50 wt %) blend films. This result also indicates that the prompt formation is closely related to the interface area. We therefore assign the prompt formation to the polaron generation from hot excitons generated near the interface of RR-P3HT/PCBM. The rate constant of the prompt polaron formation ($>10^{13}$ s^{-1}) is 10^4 times larger than the deactivation rate constant (3.0×10^9 s^{-1}) of singlet excitons in RR-P3HT pristine films. Thus, the charge-transfer efficiency (η_{CT}) is estimated to be ~100% at the P3HT/PCBM interface. On the other hand, as shown in Figure 7, the time constant of the delayed formation of polarons decreases with increasing PCBM concentration and slightly increases after thermal annealing of RR-P3HT/PCBM(50 wt %) blend films. We therefore assign the delayed formation to the polaron generation via exciton migration to the interface of RR-P3HT/PCBM. In other words, the time constant of the delayed formation of polarons is limited by exciton migration in RR-P3HT domains. Therefore, the exciton diffusion efficiency can be calculated by $\eta_{ED} = k_q/(k_F + k_q)$. In this equation, the quenching rate is calculated by $k_q = \tau_{av}^{-1} - k_F$, where τ_{av} is the averaged lifetime of singlet excitons in blend films and k_F is the deactivation rate (3.0×10^9 s^{-1}) of singlet excitons in RR-P3HT pristine films. For RR-P3HT/PCBM(50 wt %) blend films, η_{ED} is estimated to be 93% before thermal annealing and 89% after thermal annealing. In either case, η_{ED} is still high enough to collect singlet excitons into the interface of RR-P3HT/PCBM.

We now focus our attention to the charge generation in RR-P3HT/PCBM(50 wt %) blend films after thermal annealing. As shown in Figure 5, half of the polarons are promptly generated on a time scale of <100 fs, and the other half are generated on a time scale of tens of picoseconds upon excitation at 400 nm, which can excite both amorphous and crystalline domains. On the other hand, there is only one pathway for polaron generation upon excitation at 600 nm, which can selectively excite crystalline domains. The typical widths of RR-P3HT domains have been reported to be 13−15 nm.[21−23] Therefore, as shown in Scheme 1, we speculate that the 400-nm excitation can generate singlet excitons both at the relatively disordered interface and at the core crystalline region, while the 600-nm excitation can generate singlet excitons only at the core crystalline region. We have previously reported that the delocalization radius of singlet excitons is 4.3 nm[33] in RR-P3HT pristine films upon excitation at 400 nm. Considering the delocalization radius of singlet excitons and typical widths of RR-P3HT domains, it is reasonable that half of the singlet excitons promptly convert to polarons immediately after 400-nm excitation. On the other hand, the delayed polaron formation has a rise constant of 8 ps. The diffusion constant (D) of singlet excitons has been reported to be 1.8×10^{-3} cm^2 s^{-1} for RR-P3HT pristine films.[53] Therefore, the diffusion length (L_D) of singlet excitons at 8 ps is estimated to be as short as ~2 nm,[54] comparable to the remaining radius of the core crystalline region of ~2−3 nm. Note that the delocalization radius of singlet excitons is 6.7 nm[33] in the core RR-P3HT crystals. The charge generation mechanism is summarized in Scheme 2.

3.3. Charge Recombination and Dissociation. In RRa-P3HT/PCBM(50 wt %) blend films, as shown in the Supporting Information (Figure S3), the decay dynamics of transient species (PCBM anion, RRa-P3HT polarons, and RRa-P3HT photobleaching) can be fitted with a sum of an exponential function and a constant fraction and is independent of the excitation intensities ranging from 6 to 120 μJ cm^{-2}, suggesting that the dominant decay mechanism is the geminate recombination of bound radical pairs formed at the interface of RRa-P3HT and PCBM. As shown in Figure 3, ~70% of the polarons geminately

(50) Cook, S.; Furube, A.; Katoh, R. *Energy Environ. Sci.* **2008**, *1*, 294–299.
(51) Sheng, C.-X.; Tong, M.; Singh, S.; Vardeny, Z. V. *Phys. Rev. B* **2007**, *75*, 085206.
(52) Piris, J.; Kopidakis, N.; Olson, D. C.; Shaheen, S. E.; Ginley, D. S.; Rumbles, G. *Adv. Funct. Mater.* **2007**, *17*, 3849–3857.
(53) Shaw, P. E.; Ruseckas, A.; Samuel, I. D. W. *Adv. Mater.* **2008**, *20*, 3516–3520.
(54) The excitons diffusion length (L_D) of singlet excitons at 8 ps (t) is calculated by $L_D = (2Dt)^{0.5}$.

recombine to the ground state with a time constant of ~800 ps, consistent with a literature value of 800 ps for a P3HT/PCBM blend film with a low regioregularity.[28] On the other hand, the remaining ~30% of the polarons exhibit no decay on a time scale of nanoseconds. We therefore ascribed the constant fraction to dissociated polarons in RRa-P3HT/PCBM blend films. In other words, the charge dissociation efficiency (η_{CD}) is estimated to be 31%.

In RR-P3HT/PCBM(50 wt %) blend films, as shown in the Supporting Information (Figure S4), the transient signals of P3HT polarons decay faster with increasing excitation intensity at higher excitation intensities (>12 μJ cm^{-2}), indicating the bimolecular recombination of free polarons. Remarkably, no decay is observed for polaron bands at 700 and 1000 nm at lower excitation intensities (<12 μJ cm^{-2}). We therefore conclude that all of the polarons at 700 and 1000 nm are ascribed to dissociated free polarons on a time scale of nanoseconds. In other words, the direct charge dissociation efficiency (η_{CD}^{D}) is estimated to be as high as ~100% for these two polarons. Such a high dissociation efficiency is in contrast to that of RRa-P3HT/PCBM blend films. Most recently, Durrant has theoretically estimated the effective Coulomb capture radius to be ~4 nm at a typical donor/acceptor heterojunction by considering the change in entropy associated with changing from a single exciton to two separated charges.[55] Interestingly, this effective Coulomb capture radius is consistent with our estimations of the delocalization radius of singlet excitons: singlet excitons with a radius of ~4.3−6.7 nm[33] in RR-P3HT pristine films can be effectively dissociated into free polarons, while singlet excitons with a radius of ~3.2 nm[33] in RRa-P3HT pristine films form bound radical pairs. We therefore conclude that the longer separation distance of bound radical pairs >4 nm and desirable phase-separated structures in RR-P3HT/PCBM(50 wt %) blend films can promote the dissociation of bound radical pairs and the formation of free polarons effectively, whereas the shorter separation distance of bound radical pairs <4 nm and homogeneously mixed blend structures in RRa-P3HT/PCBM(50 wt %) blend films result in a significant loss due to the geminate recombination of bound radical pairs at the interface. Furthermore, the high charge mobility in RR-P3HT/PCBM(50 wt %) blend films can also lead to the dissociation of bound radical pairs effectively.[56,57]

We further focus on the deactivation of localized polarons bound to PCBM anions at 850 nm in amorphous domains of RR-P3HT. As shown in Figure 7, the localized polaron band at 850 nm, the photobleaching band of amorphous P3HT at 480 nm, and the photobleaching band of crystalline P3HT at 610 nm all have the same decay or rise constant: 500 ps before thermal annealing, 250 ps after thermal annealing. This time constant is ascribed to the hole transfer from amorphous to crystalline domains. Thus the increase in the hole-transfer rate is likely to be due to a higher hole mobility after thermal annealing.[58−60] We therefore conclude that some of localized bound radical pairs in amorphous domains can be dissociated into crystalline domains in RR-P3HT by hole transfer in competition with the geminate charge recombination (see the Supporting Information). The charge dissociation efficiency (η_{CD}^{HT}) of the hole transfer from amorphous to crystalline domains is roughly estimated by

$$\eta_{CD}^{HT} = (k_{HT} - k_{GCR})/k_{HT} \quad (1)$$

where k_{HT} is the hole-transfer rate (before thermal annealing 2×10^9 s^{-1}, after thermal annealing 4×10^9 s^{-1}) and k_{GCR} is the geminate recombination rate (1.25×10^9 s^{-1}). Thus, the charge dissociation efficiency for all the polarons is given by

$$\eta_{CD} = \frac{n_{(700\ nm)}\eta_{CD}^{D} + n_{(850\ nm)}\eta_{CD}^{HT} + n_{(1000\ nm)}\eta_{CD}^{D}}{n_{(700\ nm)} + n_{(850\ nm)} + n_{(1000\ nm)}} \quad (2)$$

where n is the relative density of each polaron, as shown in Figure 8.

As summarized in Table 1, η_{CD} is estimated to be ~31% for RRa-P3HT/PCBM(50 wt %) blend films, which is comparable to the charge dissociation efficiency by the hole-transfer $\eta_{CD}^{HT} = 38\%$ for RR-P3HT/PCBM(50 wt %) blend films before thermal annealing. This agreement is consistent with our assignment of localized bound radical pairs in amorphous domains in RR-P3HT. Interestingly, this efficiency increases from 38 to 69% after thermal annealing, suggesting that localized bound radical pairs are more efficiently dissociated into free polarons. This finding indicates that the charge dissociation of bound radical pairs is strongly dependent on the crystallinity of P3HT. These findings are consistent with a recent study that the radiative geminate recombination of bound radical pairs is more efficient for RRa-P3HT/PCBM blend films: RR-P3HT/PCBM blend films exhibit very weak charge-transfer emission, while RRa-P3HT/PCBM blend films exhibit relatively strong charge-transfer emission.[32] Furthermore, η_{CD} for RR-P3HT/PCBM(50 wt %) blend films is as high as 80% before thermal annealing and increases to 93% after thermal annealing, which is 3 times larger than that for RRa-P3HT/PCBM(50 wt %) blend films. As mentioned above, the high dissociation efficiency is mainly ascribed to large separation of bound radical pairs, desirable phase-separated networks, and high charge mobility in RR-P3HT/PCBM(50 wt %) blend films. All these conditions would assist bound radical pairs to escape from the Coulomb potential.

Table 1. Efficiencies of Fundamental Photovoltaic Conversion Processes in P3HT/PCBM(50 wt %) Solar Cells[a]

blend films	η_{ED}	η_{CT}	η_{CD}^{HT}	η_{CD}[b]	η_{CC}	IQE[c]
RRa-P3HT/PCBM	1	1		0.31	0.15	5%[61]
RR-P3HT/PCBM before annealing	0.93	1	0.38	0.80	0.57−0.74	42−55%[18,30]
RR-P3HT/PCBM after annealing	0.89	1	0.69	0.93	0.91−1	75−83%[18,30,62]

[a] η_{ED}, efficiency for singlet exciton diffusion to the P3HT/PCBM interface; η_{CT}, charge-transfer efficiency at the P3HT/PCBM interface; η_{CD}^{HT}, hole-transfer efficiency; η_{CD}, charge dissociation efficiency (the efficiency for free carrier formation); η_{CC}, charge collection efficiency; IQE, internal quantum efficiency for photovoltaic conversion. For photovoltaic conversion in polymer solar cells, the IQE can be represented by eq 3. [b] The charge dissociation efficiency is evaluated by eq 2. [c] The IQE at 400 nm is directly taken from ref 62 or evaluated by IQE = EQE/η_A, where EQE is the external quantum efficiency at 400 nm and η_A is estimated from twice the absorption at 400 nm under the following assumptions:[10] (a) 4% incident light loss at the air/glass interface and (b) 100% reflection of the Al electrode.

(55) Clarke, T. M.; Durrant, J. R. *Chem. Rev.* **2010**, DOI: 10.1021/cr900271s.
(56) Wojcik, M.; Tachiya, M. *J. Chem. Phys.* **2009**, *130*, 14107.
(57) Braun, C. L. *J. Chem. Phys.* **1984**, *80*, 4157–4161.
(58) Savenije, T. J.; Kroeze, J. E.; Yang, X.; Loos, J. *Adv. Funct. Mater.* **2005**, *15*, 1260–1266.
(59) Mihailetchi, V. D.; Xie, H.; de Boer, B.; Koster, L. J. A.; Blom, P. W. M. *Adv. Funct. Mater.* **2006**, *16*, 699–708.
(60) von Hauffa, E.; Parisi, J.; Dyakonov, V. *J. Appl. Phys.* **2006**, *100*, 043702.
(61) Campoy-Quiles, M.; Kanai, Y.; El-Basaty, A.; Sakai, H.; Murata, H. *Org. Electron.* **2009**, *10*, 1120–1132.

3.4. Charge Collection. For photovoltaic conversion in polymer solar cells, the internal quantum efficiency (IQE) can be represented by the product of each efficiency in the following fundamental processes: exciton diffusion to the donor/acceptor interface (η_{ED}), charge transfer at the interface (η_{CT}), charge dissociation into free carriers (η_{CD}), and charge collection to the electrodes (η_{CC}).

$$\mathrm{IQE} = \eta_{ED}\,\eta_{CT}\,\eta_{CD}\,\eta_{CC} \tag{3}$$

As described above, we evaluate η_{ED}, η_{CT}, and η_{CD} from the transient study. The IQE values are obtained from previous studies[18,61,62] as listed in Table 1. Thus, the charge collection efficiency η_{CC} can be estimated to be 15% for RRa-P3HT/PCBM solar cells, 57−74% for RR-P3HT/PCBM solar cells before thermal annealing, and nearly 100% for RR-P3HT/PCBM solar cells after thermal annealing. Note that these efficiencies are not absolute but should depend on the film morphology. Indeed, the difference in the IQE is probably due to the different film morphology. Nonetheless, the efficiencies listed in the table demonstrate which process is dominant to the device performance qualitatively. As shown in the inset of Figure 1b, the exponent of the power-law decay is 0.35 for RRa-P3HT/PCBM blend films, while it is 0.40 and 0.49 for RR-P3HT/PCBM blend films before and after thermal annealing, respectively (see the Supporting Information). Previously, the exponent has been reported to be around 0.3−0.7 for other P3HT/PCBM blends with different PCBM fractions or under different annealing conditions.[14,36,63,64] The larger exponent is indicative of a higher carrier mobility for the blend film.[34,35] Indeed, the hole mobility is expected to be $<10^{-5}$ cm^2 V^{-1} s^{-1} for RRa-P3HT/PCBM blend films, because it has been reported to be $\sim10^{-5}$ cm^2 V^{-1} s^{-1} for RRa-P3HT pristine films.[49] On the other hand, the hole mobility has been reported to be $\sim10^{-4}$ cm^2 V^{-1} s^{-1} for RR-P3HT/PCBM blend films before thermal annealing and 3×10^{-3} cm^2 V^{-1} s^{-1} for RR-P3HT/PCBM blend films after thermal annealing.[59] We therefore conclude that the remarkable difference in the charge collection efficiency is closely related to the carrier mobility of blend films.

3.5. Relevance to Device Performance of Polymer Solar Cells. Finally, we summarize the fundamental processes for RRa-P3HT/PCBM and RR-P3HT/PCBM blend films and discuss the relevance of these fundamental processes to the device performance of polymer solar cells, as illustrated in Scheme 2. First, we note that the exciton diffusion efficiency η_{ED} is as high as ∼100% for RRa-P3HT/PCBM(50 wt %) blend films and 93% for RR-P3HT/PCBM(50 wt %) blend films before thermal annealing, which slightly decreases to 89% after thermal annealing. In other words, homogeneously mixed blend structures of RRa-P3HT/PCBM(50 wt %) films are preferable to phase-separated blend structures of RR-P3HT/PCBM(50 wt %) films in terms of the exciton collection to the interface. This is consistent with the PL quenching experiments, indicating that there is room to further improve the exciton diffusion efficiency in RR-P3HT/PCBM, as reported by Schwartz.[65] We note that the difference is not so large. Second, the charge-transfer efficiency η_{CT} is as high as ∼100% for both RRa-P3HT/PCBM(50 wt %) and RR-P3HT/PCBM(50 wt %) blend films, suggesting that it is dependent on the combination of donor and acceptor materials rather than blend structures. Third, the charge dissociation efficiency η_{CD} is as low as ∼30% for RRa-P3HT/PCBM(50 wt %) blend films, while it is as high as 80% for RR-P3HT/PCBM(50 wt %) blend films before thermal annealing and 93% for RR-P3HT/PCBM(50 wt %) blend films after thermal annealing. Fourth, furthermore, the charge collection efficiency η_{CC} is only 15% for RRa-P3HT/PCBM(50 wt %) blend films, while it is 57−74% for RR-P3HT/PCBM(50 wt %) blend films before thermal annealing and as high as 91−100% for RR-P3HT/PCBM(50 wt %) blend films after thermal annealing. The significant differences in η_{CD} and η_{CC} are mainly ascribed to the phase-separated networks and the crystallization of RR-P3HT, resulting in improved carrier mobility and large separation of bound radical pairs. The high charge collection efficiency is consistent with previous reports that the short-circuit current density (J_{SC}) in RR-P3HT/PCBM solar cells increases linearly with increasing irradiation intensity up to 1 sun, suggesting that the bimolecular recombination loss is negligible.[66] Recent studies also have shown that the bimolecular recombination rate in RR-P3HT/PCBM blend films is 2 orders of magnitude lower than the Langevin recombination rate in homogeneous structures.[43,64,67] On the basis of these analyses, we emphasize that there is not much difference in the charge generation yield between RRa-P3HT/PCBM(50 wt %) and RR-P3HT/PCBM(50 wt %) blend films. Rather, the charge dissociation and collection have a critical impact on the device performance of P3HT/PCBM solar cells. The desirable phase-separated network structures,[21−23] which have been recently revealed by 3D TEM tomography, play a crucial role in the high efficiency of the charge dissociation and collection.

4. Conclusions

We have comprehensively studied fundamental photovoltaic conversion processes in RRa-P3HT/PCBM and RR-P3HT/PCBM blend films—exciton diffusion to the donor/acceptor interface, charge transfer at the interface, charge dissociation into free carriers, and charge collection to the electrode—by transient absorption spectroscopy in the wavelength region from 450 to 1650 nm under various excitation intensities and different excitation wavelengths. On the basis of these detailed analyses, we obtained all of the efficiencies of these fundamental processes that are related to blend structures of P3HT and PCBM. For RRa-P3HT/PCBM(50 wt %) blend films, the efficiency was evaluated to be 100% for exciton diffusion (η_{ED}), 100% for charge transfer (η_{CT}), 31% for charge dissociation (η_{CD}), and 15% for charge collection (η_{CC}). The η_{ED} as high as 100% is attributed to relatively homogeneously mixed blend structures of RRa-P3HT/PCBM, which would result in an intermolecular distance of PCBM molecules shorter than the delocalization radius of singlet excitons (3.2 nm). At the P3HT/PCBM interface, the charge-transfer efficiency η_{CT} is as high as 100% with a time constant of <0.2 ps. In other words, all of the singlet excitons can be converted into bound radical pairs. However, the charge dissociation efficiency η_{CD} is as small as 31% for this blend film, because most of the bound radical pairs

(62) Takanezawa, K.; Tajima, K.; Hashimoto, K. *Appl. Phys. Lett.* **2008**, *93*, 063308.
(63) Clarke, T. M.; Jamieson, F. C.; Durrant, J. R. *J. Phys. Chem. C* **2009**, *113*, 20934–20941.
(64) Shuttle, C. G.; O'Regan, B.; Ballantyne, A. M.; Nelson, J.; Bradley, D. D. C.; Durrant, J. R. *Phys. Rev. B* **2008**, *78*, 113201.
(65) Ayzner, A. L.; Wanger, D. D.; Tassone, C. J.; Tolbert, S. H.; Schwartz, B. J. *J. Phys. Chem. C* **2008**, *112*, 18711–18716.
(66) Schilinsky, P.; Waldauf, C.; Brabec, C. J. *Appl. Phys. Lett.* **2002**, *81*, 3885–3887.
(67) Sliaužys, G.; Juška, G.; Arlauskas, K.; Pivrikas, A.; Österbacka, R.; Scharber, M.; Mozer, A.; Sariciftci, N. S. *Thin Solid Films* **2006**, *511−512*, 224–227.

geminately recombine to the ground state. Furthermore, the charge collection efficiency η_{CC} is only 15%. The low efficiencies of η_{CD} and η_{CC} are partly due to homogeneously mixed blend structures, which are likely to cause the geminate recombination. In these structures, highly disordered localized polarons would cause lower carrier mobility, resulting in lower charge collection efficiency. In other words, homogeneously mixed blend structures of RRa-P3HT/PCBM are desirable in η_{ED} but crucially disadvantageous in η_{CD} and η_{CC}. For RR-P3HT/PCBM(50 wt %) blend films, each efficiency was evaluated to be 93% for η_{ED}, 100% for η_{CT}, 80% for η_{CD}, and 57−74% for η_{CC} before thermal annealing and 89% for η_{ED}, 100% for η_{CT}, 93% for η_{CD}, and 91−100% for η_{CC} after thermal annealing. The time constant of the exciton diffusion is of the order of tens of picoseconds, which depends on the phase-separated structures in the blend films. The charge transfer at the interface occurs on a time scale of <100 fs with an efficiency as high as 100%. Interestingly, there are two pathways for charge generation in RR-P3HT/PCBM blend films upon excitation at 400 nm, which can excite both amorphous and crystalline domains: half of the polarons are promptly generated on a time scale of <100 fs, and the other half are generated on a time scale of tens of picoseconds upon excitation at 400 nm. On the other hand, there is only one pathway for polaron generation upon excitation at 600 nm, which can selectively excite crystalline domains. The prompt formation is assigned to polaron generation from hot excitons generated near the interface of RR-P3HT/PCBM. The delayed formation is assigned to polaron generation via exciton migration to the interface of RR-P3HT/PCBM. For RR-P3HT/PCBM(50 wt %) blend films, three polaron bands are observed at 700, 850, and 1000 nm and assigned to delocalized polarons, localized bound polarons, and localized polarons, respectively. We speculate that delocalized polarons at 700 nm are located in fibrillar networks of P3HT crystals, localized polarons at 1000 nm are located in disordered P3HT matrices, and localized polarons at 850 nm are loosely bound to PCBM at the interface in disordered amorphous P3HT matrices. Polarons at 700 and 1000 nm are directly dissociated into free carriers with η_{CD}^{D} as high as 100%. On the other hand, loosely bound radical pairs at 850 nm are partly dissociated into free carriers by the hole transfer from amorphous to crystalline domains with η_{CD}^{HT} of 38% before thermal annealing and η_{CD}^{HT} of 69% after thermal annealing. From these efficiencies and reported IQE values, η_{CC} is estimated to be 57−74% before thermal annealing and nearly 100% after thermal annealing. In summary, there is little difference in the charge generation yield between RRa-P3HT/PCBM(50 wt %) and RR-P3HT/PCBM(50 wt %) blend films. Rather, the charge dissociation and collection have a critical impact on the device performance of P3HT/PCBM solar cells. The high dissociation efficiency is mainly ascribed to large separation of bound radical pairs, desirable phase-separated networks, and high charge mobility in RR-P3HT/PCBM(50 wt %) blend films. We note that there is still room to further improve the exciton diffusion efficiency in RR-P3HT/PCBM solar cells. Our findings provide experimental evidence of molecular understanding of photovoltaic conversion processes that is closely related to phase-separated structures in the active layer.

Acknowledgment. This work was partly supported by Kansai Research Foundation for technology promotion, the JST PRESTO program, and the Global COE program (International Center for Integrated Research and Advanced Education in Materials Science) from the Ministry of Education, Culture, Sports, Science, and Technology, Japan.

Supporting Information Available: Details about the sample preparation, measurements, steady-state absorption spectra, PL quenching results of P3HT/PCBM blend films, excitation intensity dependence of singlet exciton decay in RRa-P3HT/PCBM(50 wt %) blend films, excitation intensity dependence for charge recombination in P3HT/PCBM(50 wt %) blend films, dynamic and spectral analyses of transient absorption, transient absorption spectra and decay of RR-P3HT/PCBM(50 wt %) blend films in microsecond time domains, and the relative energy levels for polarons generated in P3HT/PCBM blend films and their transition energies. This material is available free of charge via the Internet at http://pubs.acs.org.

JA100302P